Convenient Access to Functionalized Non-Symmetrical Atropisomeric 4,4'-Bipyridines

Emmanuel Aubert, Emmanuel Wenger, Paola Peluso, Victor Mamane

compounds

MDPI

Article

Convenient Access to Functionalized Non-Symmetrical Atropisomeric 4,4′-Bipyridines

Emmanuel Aubert [1], Emmanuel Wenger [1], Paola Peluso [2,*] and Victor Mamane [3,*]

[1] CNRS, CRM2, Université de Lorraine, F-54000 Nancy, France; emmanuel.aubert@univ-lorraine.fr (E.A.); emmanuel.wenger@univ-lorraine.fr (E.W.)
[2] Institute of Biomolecular Chemistry ICB, CNR, Secondary Branch of Sassari, Traversa La Crucca 3, Regione Baldinca, Li Punti, 07100 Sassari, Italy
[3] Strasbourg Institute of Chemistry, UMR CNRS 7177, Team LASYROC, 1 Rue Blaise Pascal, University of Strasbourg, 67008 Strasbourg, France
* Correspondence: paola.peluso@cnr.it (P.P.); vmamane@unistra.fr (V.M.); Tel.: +39-079-2841218 (P.P.); +33-3-68851612 (V.M.)

Abstract: Non-symmetrical chiral 4,4′-bipyridines have recently found interest in organocatalysis and medicinal chemistry. In this regard, the development of efficient methods for their synthesis is highly desirable. Herein, a series of non-symmetrical atropisomeric polyhalogenated 4,4′-bipyridines were prepared and further functionalized by using cross-coupling reactions. The desymmetrization step is based on the *N*-oxidation of one of the two pyridine rings of the 4,4′-bipyridine skeleton. The main advantage of this methodology is the possible post-functionalization of the pyridine *N*-oxide, allowing selective introduction of chlorine, bromine or cyano groups in 2- and 2′-postions of the chiral atropisomeric 4,4′-bipyridines. The crystal packing in the solid state of some newly prepared derivatives was analyzed and revealed the importance of halogen bonds in intermolecular interactions.

Keywords: atropisomerism; 4,4′-bipyridine; pyridine *N*-oxidation; halogenation; halogen bond; cyanation; Finkelstein reaction; Suzuki coupling

Citation: Aubert, E.; Wenger, E.; Peluso, P.; Mamane, V. Convenient Access to Functionalized Non-Symmetrical Atropisomeric 4,4′-Bipyridines. *Compounds* **2021**, *1*, 58–74. https://doi.org/10.3390/compounds1020006

Academic Editor: Juan Mejuto

Received: 19 April 2021
Accepted: 31 May 2021
Published: 1 July 2021

1. Introduction

4,4′-Bipyridines are useful ligands for the design of coordination polymers and metal-organic frameworks (MOFs) [1], and are key components in the preparation of viologens [2,3]. In contrast to 2,2′-bipyridines for which a large number of chiral derivatives were developed [4–6], chiral 4,4′-bipyridines were much less explored. In the latter derivatives, the chirality can be brought by specific functions on the pyridine rings [7,8] or by atropisomery [9,10]. Indeed, atropisomeric 4,4′-bipyridines are the particular case where rotation around the pyridyl-pyridyl bond is blocked by the presence of three or four substituents. They were first used for the preparation of metallo-supramolecular squares [9] and some years later for building chiral MOFs [11]. These last years, our groups were involved in the development of halogenated chiral 4,4′-bipyridines and in the study of their performances as halogen- [12,13] and chalcogen [14,15] bond donors in different applications such as organocatalysis [16] and medicinal chemistry [17].

Particularly, we have shown that homocoupling reactions represent straightforward ways for the synthesis of symmetrical chiral 4,4′-bipyridines [10,18]. However, these methods are not relevant for the synthesis of the non-symmetrical derivatives; therefore, desymmetrization processes have to be employed. Very limited methods for the desymmetrization of the 4,4′-bipyridine framework to non-symmetrical chiral 4,4′-bipyridines were reported. During their work on the 3,3′-dilithiation of octachloro-4,4′-bipyridine **1**, Foulger and Wakefield observed that quenching with dichlorodiphenylsilane and di-π-cyclopentadienyltitanium dichloride generated 4,4′-bipyridines **2** and **3**, respectively [19] (Figure 1a). Later, we showed that 3-mono- and 3,5′-dilithiation of 2,2′-dibromo-5,5′-dichloro-4,4′-bipyridine **4** and subsequent electrophilic trapping furnished 4,4′-bipyridines

5 and **6**, respectively [20] (Figure 1b). Finally, very recently, we used lithiation and cross-coupling reactions in 2-position of 2,2′-diiodo-3,3′,5,5′-tetrachloro-4,4′-bipyridine **7** as non-selective routes to 4,4′-bipyridines **8** and **9** [17] (Figure 1c). It is worth mentioning that in all these examples the yields were low to moderate.

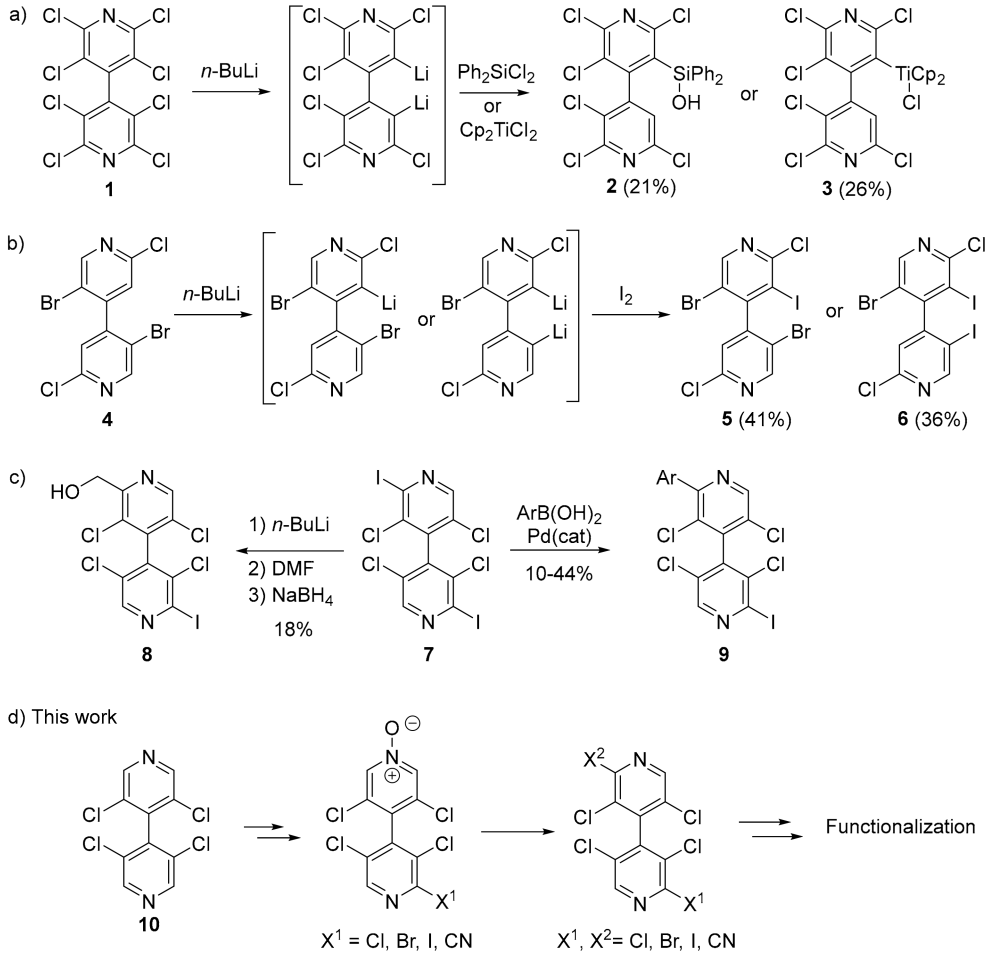

Figure 1. Non-symmetrical chiral 4,4′-bipyridines obtained by desymmetrization of parent 4,4′-bipyridines in the literature (**a**–**c**) and in the present work (**d**).

Herein, the *N*-oxidation as a straightforward and operatively easy method was used to desymmetrize 3,3′,5,5′-tetrachloro-4,4′-bipyridine **10**. The advantage of the reported methodology relies on the chemical transformations allowed by the pyridine N-O function, such as halogenation and cyanation [21]. The halogenated 4,4′-bipyridines were further functionalized through metal-catalyzed coupling reactions (Figure 1d). Moreover, X-ray diffraction analysis of selected compounds revealed very interesting solid-state packing features.

2. Materials and Methods

2.1. General Information

Proton (^{1}H NMR) and carbon (^{13}C NMR) nuclear magnetic resonance spectra were recorded on a Bruker Avance III instrument operating at 300, 400, or 500 MHz (Bruker Corporation, Billerica, MA, USA). The chemical shifts are given in parts per million (ppm) on the delta scale. The solvent peak was used as reference values for ^{1}H NMR ($CDCl_3$ = 7.26 ppm) and for ^{13}C NMR ($CDCl_3$ = 77.16 ppm). Data are presented as follows: Chemical shift, multiplicity (s = singlet, d = doublet, t = triplet, q = quartet, quint = quintet, m = multiplet, b = broad), integration, and coupling constants (J/Hz). High-resolution mass spectra (HRMS) data were recorded on a micrOTOF spectrometer (Bruker Corporation,

Billerica, MA, USA) equipped with an orthogonal electrospray interface (ESI). Analytical thin layer chromatography (TLC plates from Merck KGaA, Darmstadt, Germany) was carried out on silica gel 60 F254 plates with visualization by ultraviolet light. Reagents and solvents were purified using standard means. Tetrahydrofuran (THF) was distilled from sodium metal/benzophenone and freshly used. Dry dichloromethane was obtained by passing through activated alumina under a positive pressure of argon using GlassTechnology GTS100 devices. Dry dioxane (over molecular sieve) was purchased from Aldrich, triethylamine and diisopropylamine were distilled over CaH_2 and stored over KOH under an argon atmosphere. Anhydrous reactions were carried out in flame-dried glassware and under an argon atmosphere. All other chemicals were used as received.

2.2. Syntheses

2.2.1. 3,3′,5,5′-Tetrachloro-4,4′-Bipyridine **10**

To a solution of diisopropylamine (27.5 mmol, 3.85 mL) in THF (200 mL) at −40 °C was added a solution of *n*-BuLi (1.6 M in hexanes, 27.5 mmol, 17.2 mL) and the mixture was stirred for 20 min. A solution of 3,5-dichloropyridine **11** (50 mmol, 7.4 g) in THF (100 mL) was added during 1 h while maintaining the temperature close to −40 °C. The temperature of the cloudy solution was slowly raised to −15 °C (during 1h) to give a homogeneous dark red solution. The temperature was lowered to −78 °C then a solution of I_2 (30 mmol, 7.62 g) in THF (50 mL) was slowly added. After 10 min at −78 °C, the temperature was raised to room temperature and the reaction was quenched by the addition of aqueous saturated solution of $Na_2S_2O_3$ (100 mL). Water was added (200 mL) and the mixture was extracted three times with ethyl acetate (3 × 200 mL). The organic phases were combined, washed with brine (100 mL) and dried over $MgSO_4$. After concentration, the crude compound was purified by chromatography on silica gel (cyclohexane/ethyl acetate 95/5) to give 4,4′-bipyridine **10** (3.64 g) and compound **12** (2.7 g). Compound **12** was diluted with ethyl acetate (200 mL) and I_2 (18 mmol, 4.57g) was added and the mixture was stirred overnight at room temperature in an open flask. The reaction was quenched by the addition of aqueous saturated solution of $Na_2S_2O_3$ (25 mL). Water was added (50 mL) and the organic phases washed with brine (100 mL) and dried over anhydrous $MgSO_4$. After concentration, the crude compound was purified by chromatography on silica gel (cyclohexane/ethyl acetate 95/5) to give 4,4′-bipyridine **10** (2.4 g). A total mass of 6.04 g of **10** was obtained which corresponds to an overall yield of 82%. The NMR data for **10** are in complete agreement with the literature [22].

3,3′,5,5′-Tetrachloro-1,4-dihydro-4,4′-bipyridine (**12**). Yellow solid, mp 155–157 °C. ^{1}H NMR (500 MHz, CD_3COCD_3) δ 8.57 (s, 1H), 8.56 (s, 1H), 7.55 (s, 1H, NH), 6.56 (s, 1H), 6.55 (s, 1H), 5.87 (s, 1H). ^{13}C NMR (126 MHz, CD_3COCD_3) δ 150.7, 148.3, 142.5, 134.3, 134.0, 127.7, 102.8, 50.6. HRMS (ESI-TOF) $[M + H]^+$ *m/z*: Calcd. for $C_{10}H_6Cl_5N_2$ 294.9285, found: 294.9327 (Figure S1).

2.2.2. 3,3′,5,5′-Tetrachloro-[4,4′-Bipyridine] 1-Oxide **13**

4,4′-Bipyridine **10** (12.38 mmol, 3.64 g) was dissolved in CH_2Cl_2 (62 mL) at room temperature. *m*-CPBA (*m*-chloro-perbenzoic acid) (77% purity, 12.38 mmol, 2.8 g) was added and the mixture was stirred for 24 h. After dilution with CH_2Cl_2 (140 mL), the mixture was washed with NaOH 1M (2 × 100 mL) and with brine. The organic phase was dried over $MgSO_4$, concentrated and purified by chromatography on silica gel (CH_2Cl_2/methanol 99/1) to give respectively the starting compound **10** (850 mg, 23%), compound **13** (2.0 g, 54% Yield) and the bis *N*-oxide **14** (925 mg, 23%).

3,3′,5,5′-Tetrachloro-[4,4′-bipyridine] 1-oxide (**13**). White solid, mp 218–220 °C. ^{1}H NMR (500 MHz, $CDCl_3$) δ 8.68 (s, 2H), 8.31 (s, 2H). ^{13}C NMR (126 MHz, $CDCl_3$) δ 148.0, 139.0, 138.3, 132.9, 132., 130.2. HRMS (ESI-TOF) $[M + H]^+$ *m/z*: Calcd. for $C_{10}H_5Cl_4N_2O$ 308.9150, found: 308.9153 (Figure S2).

3,3′,5,5′-Tetrachloro-[4,4′-bipyridine] 1,1′-dioxide (**14**). White solid, mp 270–272 °C. ^{1}H NMR (500 MHz, $CDCl_3$) δ 8.31 (s, 4H). ^{13}C NMR (126 MHz, $CDCl_3$) δ 138.3, 133.7, 128.9.

HRMS (ESI-TOF) $[M + H]^+$ *m/z*: Calcd. for $C_{10}H_5Cl_4N_2O_2$ 324.9100, found: 324.9095 (Figure S3).

2.2.3. 2-Bromo-3,3′,5,5′-Tetrachloro-4,4′-Bipyridine **15**

3,3′,5,5′-Tetrachloro-[4,4′-bipyridine] 1-oxide **13** (6.37 mmol, 1.91 g) was dissolved in dibromoethane (15 mL) and triethylamine (12.73 mmol, 1.7 mL) was added. The mixture was cooled to −40 °C and oxalyl bromide (12.73 mmol, 1.8 mL) was slowly added while maintaining the temperature below −35 °C. After stirring 1h at −40 °C, methanol (1 mL) was added and temperature was raised to room temperature. A saturated solution of ammonium chloride (20 mL) was added and the mixture was extracted with CH_2Cl_2 (3 × 50 mL). The organic phase was dried over $MgSO_4$, filtered and concentrated under vacuum. The crude compound was purified by chromatography on silica gel (pentane/CH_2Cl_2 7/3 to 2/1) to give pure 4,4′-bipyridine **15** (2.18 g, 94% yield). White solid, mp 100–102 °C. ^{1}H NMR (500 MHz, $CDCl_3$) δ 8.68 (s, 2H), 8.48 (s, 1H). ^{13}C NMR (126 MHz, $CDCl_3$) δ 148.1, 147.2, 142.1, 140.7, 140.4, 132.9, 130.9, 130.6. HRMS (ESI-TOF) $[M + H]^+$ *m/z*: Calcd. for $C_{10}H_4BrCl_4N_2$ 370.8306, found: 370.8302 (Figure S4).

2.2.4. 3,3′,5,5′-Tetrachloro-[4,4′-Bipyridine]-2-Carbonitrile **16**

3,3′,5,5′-Tetrachloro-[4,4′-bipyridine] 1-oxide **13** (1 mmol, 310 mg) was dissolved in acetonitrile (2 mL) and triethylamine (0.5 mL). Trimethylsilylcyanide (3 mmol, 375 µL) was slowly added and the mixture was refluxed at 100 °C for 24 h. The temperature lowered to 0 °C, a solution of NaOH (5 M, 20 mL) was slowly added and the mixture was extracted with CH_2Cl_2 (3 × 30 mL). The organic phase was dried over $MgSO_4$, filtered and concentrated under vacuum. The crude compound was purified by chromatography on silica gel (pentane/ethyl acetate 7/3) to give 4,4′-bipyridine **16** (267 mg, 83% yield). White solid, mp 99–101 °C. ^{1}H NMR (500 MHz, $CDCl_3$) δ 8.76 (s, 1H), 8.71 (s, 2H). ^{13}C NMR (126 MHz, $CDCl_3$) δ 149.1, 148.2, 141.9, 138.7, 135.40, 135.35, 132.3, 130.9. HRMS (ESI-TOF) $[M + H]^+$ *m/z*: Calcd. for $C_{11}H_3Cl_4N_3$ 317.9154, found: 317.9151 (Figure S5).

2.2.5. 2-Bromo-3,3′,5,5′-Tetrachloro-[4,4′-Bipyridine] 1-Oxide **17**

2-Bromo-3,3′,5,5′-tetrachloro-4,4′-bipyridine **15** (5.36 mmol, 2.0 g) was dissolved in CH_2Cl_2 (28 mL) at room temperature. *m*-CPBA (77% purity, 11 mmol, 2.47 g) was added and the mixture was stirred for 60 h. After dilution with CH_2Cl_2 (100 mL), the mixture was washed with NaOH 1M (2 × 80 mL) and with brine. The organic phase was dried over $MgSO_4$, concentrated and purified by chromatography on silica gel (CH_2Cl_2/methanol 99/1) to give compound **17** (1.72 g, 83%). White solid, mp 212–214 °C. ^{1}H NMR (500 MHz, $CDCl_3$) δ 8.48 (s, 1H), 8.31 (s, 2H). ^{13}C NMR (126 MHz, $CDCl_3$) δ 147.2, 141.1, 140.8, 138.4, 133.6, 132.6, 131.3, 130.4. HRMS (ESI-TOF) $[M + H]^+$ *m/z*: Calcd. for $C_{10}H_3BrCl_4N_2O$ 386.8256, found: 386.8265 (Figure S6).

2.2.6. 3,3′,5,5′-Tetrachloro-2′-Cyano-[4,4′-Bipyridine] 1-Oxide **18**

Procedure 2.2.5. was used starting from 3,3′,5,5′-tetrachloro-[4,4′-bipyridine]-2-carbonitrile **16** (0.5 mmol, 160 mg) and *m*-CPBA (77% purity, 1 mmol, 224 mg) in CH_2Cl_2 (2.5 mL). After purification by chromatography on silica gel (CH_2Cl_2/methanol 98/2), compound **18** was obtained (158 mg, 94%). White solid, mp 193–195 °C. ^{1}H NMR (500 MHz, $CDCl_3$) δ 8.78 (s, 1H), 8.32 (s, 2H). ^{13}C NMR (126 MHz, $CDCl_3$) δ 149.2, 141.0, 138.5, 136.2, 136.1, 132.7, 132.3, 128.4, 113.9. HRMS (ESI-TOF) $[M + H]^+$ *m/z*: Calcd. for $C_{11}H_3Cl_4N_3O$ 333.9103, found: 333.9091 (Figure S7).

2.2.7. 2-Bromo-2′,3,3′,5,5′-Pentachloro-4,4′-Bipyridine **19**

Procedure 2.2.3. was used starting from 2-bromo-3,3′,5,5′-tetrachloro-[4,4′-bipyridine] 1-oxide **17** (0.179 mmol, 70 mg), oxalyl chloride (0.358 mmol, 31 µL), triethylamine (0.358 mmol, 50 µL) in CH_2Cl_2 (0.5 mL). After purification by chromatography on silica gel (pentane/ethyl acetate 97/3), compound **19** was obtained (51 mg, 70%). White solid, mp

119–121 °C. ^{1}H NMR (500 MHz, $CDCl_3$) δ 8.50 (s, 1H), 8.49 (s, 1H). ^{13}C NMR (126 MHz, $CDCl_3$) δ 148.7, 147.3, 146.9, 142.9, 142.2, 140.8, 132.6, 130.3, 129.9, 129.8. HRMS (ESI-TOF) $[M + H]^+$ *m/z*: Calcd. for $C_{10}H_2BrCl_5N_2$ 404.7917, found: 404.7921 (Figure S8).

2.2.8. 2′,3,3′,5,5′-Pentachloro-[4,4′-Bipyridine]-2-Carbonitrile **20**

Procedure 2.2.3. was used starting from 3,3′,5,5′-tetrachloro-[4,4′-bipyridine]-2-carbonitrile **16** (0.179 mmol, 60 mg), oxalyl chloride (0.358 mmol, 31 µL), triethylamine (0.358 mmol, 50 µL) in CH_2Cl_2 (0.5 mL). After purification by chromatography on silica gel (pentane/ethyl acetate 95/5), compound **20** was obtained (45 mg, 71%). Colorless syrup. ^{1}H NMR (500 MHz, $CDCl_3$) δ 8.78 (s, 1H), 8.53 (s, 1H). ^{13}C NMR (126 MHz, $CDCl_3$) δ 149.2, 149.0, 147.1, 142.1, 141.2, 135.1, 132.4, 129.9, 129.7, 113.9. HRMS (ESI-TOF) $[M + H]^+$ *m/z*: Calcd. for $C_{11}H_2Cl_5N_3$ 351.8764, found: 351.8774 (Figure S9).

2.2.9. 3,3′,5,5′-Tetrachloro-2′-Iodo-[4,4′-Bipyridine] 1-Oxide **21**

In a dry tube were placed 2-bromo-3,3′,5,5′-tetrachloro-[4,4′-bipyridine] 1-oxide **17** (4.11 mmol, 1.6 g), NaI (8.22 mmol, 1.23 g), CuI (0.411 mmol, 78 mg) and (rac)-*trans*-cyclohexane-1,2-diamine (0.822 mmol, 117 mg). The tube was evacuated and filled with argon before addition of degassed dioxane (15 mL). The tube was sealed with a screw cap and heated at 120 °C for 60 h. After cooling to room temperature, NH_4OH (20 mL) and H_2O (40 mL) were added then the product was extracted with dichloromethane (3 × 50 mL). After drying over $MgSO_4$, filtration and concentration, the crude compound was purified by chromatography on silica gel (CH_2Cl_2/methanol 99/1) to give compound **21** (1.29 g, 72%). White solid, mp 244–246 °C. ^{1}H NMR (500 MHz, $CDCl_3$) δ 8.47 (s, 1H), 8.30 (s, 2H). ^{13}C NMR (126 MHz, $CDCl_3$) δ 147.8, 139.2, 138.3, 138.0, 132.6, 131.8, 130.7, 119.4. HRMS (ESI-TOF) $[M + H]^+$ *m/z*: Calcd. for $C_{10}H_3Cl_4IN_2O$ 434.8117, found: 434.8109 (Figure S10).

2.2.10. 2,3,3′,5,5′-Pentachloro-2′-Iodo-4,4′-Bipyridine **22**

Procedure 2.2.3. was used starting from 3,3′,5,5′-tetrachloro-2′-iodo-[4,4′-bipyridine] 1-oxide **21** (0.179 mmol, 78 mg), oxalyl chloride (0.358 mmol, 31 µL), triethylamine (0.358 mmol, 50 µL) in CH_2Cl_2 (0.5 mL). After purification by chromatography on silica gel (pentane/ethyl acetate 97/3), compound **22** was obtained (65 mg, 80%). White solid, mp 140–142 °C. ^{1}H NMR (500 MHz, $CDCl_3$) δ 8.48 (s, 1H), 8.49 (s, 1H). ^{13}C NMR (126 MHz, $CDCl_3$) δ 148.7, 147.9, 146.9, 143.1, 140.4, 137.0, 130.8, 129.8, 129.7, 119.5. HRMS (ESI-TOF) $[M + H]^+$ *m/z*: Calcd. for $C_{10}H_2Cl_5IN_2$ 452,7778, found: 452.7749 (Figure S11).

2.2.11. 2′-Bromo-3,3′,5,5′-Tetrachloro-[4,4′-Bipyridine]-2-Carbonitrile **23**

Procedure 2.2.3. was used starting from 3,3′,5,5′-tetrachloro-2′-cyano-[4,4′-bipyridine] 1-oxide **18** (0.297 mmol, 100 mg), oxalyl bromide (0.595 mmol, 85 µL), triethylamine (0.595 mmol, 80 µL) in CH_2Br_2 (1 mL). After purification by chromatography on silica gel (pentane/ethyl acetate 95/5), compound **23** was obtained (107 mg, 90%). White solid, mp 131–133 °C. ^{1}H NMR (500 MHz, $CDCl_3$) δ 8.77 (s, 1H), 8.52 (s, 1H). ^{13}C NMR (126 MHz, $CDCl_3$) δ 149.2, 147.4, 142.2, 141.0, 140.7, 135.06, 135.05, 132.5, 132.4, 130.2, 113.9. HRMS (ESI-TOF) $[M + H]^+$ *m/z*: Calcd. for $C_{11}H_2BrCl_4N_3$ 395.8259, found: 395.8277 (Figure S12).

2.2.12. 2-Bromo-3,3′,5,5′-Tetrachloro-2′-Iodo-4,4′-Bipyridine **24**

Procedure 2.2.3. was used starting from 3,3′,5,5′-tetrachloro-2′-iodo-[4,4′-bipyridine] 1-oxide **21** (1.74 mmol, 760 mg), oxalyl bromide (3.49 mmol, 496 µL), triethylamine (3.49 mmol, 463 µL) in CH_2Br_2 (4.2 mL). After purification by chromatography on silica gel (pentane/CH_2Cl_2 7/3), compound **24** was obtained (710 mg, 81%). White solid, mp 165–167 °C. ^{1}H NMR (500 MHz, $CDCl_3$) δ 8.414 (s, 1H), 8.410 (s, 1H). ^{13}C NMR (126 MHz, $CDCl_3$) δ 147.9, 147.3, 142.6, 140.8, 140.5, 137.0, 132.5, 130.8, 130.2, 119.5. HRMS (ESI-TOF) $[M + H]^+$ *m/z*: Calcd. for $C_{10}H_2BrCl_4IN_2$ 496.7273, found: 496.7242 (Figure S13).

2.2.13. 3,3′,5,5′-Tetrachloro-2′-Iodo-[4,4′-Bipyridine]-2-Carbonitrile **25**

Procedure 2.2.4. was used starting from 3,3′,5,5′-tetrachloro-2′-iodo-[4,4′-bipyridine] 1-oxide **21** (0.395 mmol, 172 mg), acetonitrile (1.5 mL), triethylamine (0.4 mL) and trimethylsilylcyanide (1.18 mmol, 150 µL). After purification by chromatography on silica gel (pentane/ethyl acetate 95/5), compound **25** was obtained (110 mg, 62%). White solid, mp 144–146 °C. ^{1}H NMR (500 MHz, $CDCl_3$) δ 8.77 (s, 1H), 8.51 (s, 1H). ^{13}C NMR (126 MHz, $CDCl_3$) δ 149.2, 148.0, 142.4, 138.9, 137.0, 135.1, 135.0, 132.4, 130.7, 119.7, 114.0. HRMS (ESI-TOF) $[M + H]^+$ *m/z*: Calcd. for $C_{11}H_2Cl_4IN_3$ 443.8120, found: 443.8121 (Figure S14).

2.2.14. 2-Bromo-3,3′,5,5′-Tetrachloro-2′-Phenyl-4,4′-Bipyridine **26**

In a dry tube were placed 2-bromo-3,3′,5,5′-tetrachloro-2′-iodo-4,4′-bipyridine **24** (0.3 mmol, 151.5 mg), $Pd(PPh_3)_4$ (0.015 mmol, 17.3 mg), phenylboronic acid (0.3 mmol, 36.6 mg) and K_3PO_4 (0.3 mmol, 64 mg). The tube was evacuated and filled with argon before addition of degassed mixture of toluene/water/ethanol (6:1:1, 4 mL). The tube was sealed with a screw cap and heated at 100 °C for 15 h. The cooled reaction mixture was diluted with water (10 mL) and extracted with CH_2Cl_2 (3 × 15 mL). After drying over $MgSO_4$, filtration and concentration, the crude compound was purified by chromatography on silica gel (pentane/ethyl acetate 98/2) to give compound **26** (122 mg, 89%). Colorless syrup. ^{1}H NMR (500 MHz, $CDCl_3$) δ 8.76 (s, 1H), 8.49 (s, 1H), 7.78–7.25 (m, 2H), 7.52–7.46 (m, 3H). ^{13}C NMR (126 MHz, $CDCl_3$) δ 156.2, 147.5, 147.2, 143.1, 141.7, 140.7, 137.0, 132.8, 130.6, 129.6, 129.5, 129.1, 128.7, 128.4. HRMS (ESI-TOF) $[M + H]^+$ *m/z*: Calcd. for $C_{16}H_7BrCl_4N_2$ 446.8619, found: 446.8625 (Figure S15).

2.2.15. 2-Bromo-2′-(4-((Tert-Butyldimethylsilyl)oxy)phenyl)-3,3′,5,5′-Tetrachloro-4,4′-Bipyridine **27**

Procedure 2.2.14. was used starting from 2-bromo-3,3′,5,5′-tetrachloro-2′-iodo-4,4′-bipyridine **24** (0.3 mmol, 151.5 mg), $Pd(PPh_3)_4$ (0.015 mmol, 17.3 mg), 4-((tert-butyldimethylsilyl)oxy)phenyl boronic acid (0.3 mmol, 75.7 mg) and K_3PO_4 (0.3 mmol, 64 mg). After purification by chromatography on silica gel (pentane/ethyl acetate 98/2), compound **27** was obtained (137 mg, 79%). Colorless syrup. ^{1}H NMR (500 MHz, $CDCl_3$) δ 8.72 (s, 1H), 8.49 (s, 1H), 7.69 (d, J = 8.5 Hz, 2H), 6.94 (d, J = 8.5 Hz, 2H), 1.00 (s, 9H), 0.24 (s, 6H). ^{13}C NMR (126 MHz, $CDCl_3$) δ 157.1, 155.8, 147.3, 147.2, 143.3, 141.6, 140.7, 132.9, 131.1, 130.7, 130.0, 128.5, 128.4, 120.0, 25.8, 18.4, −4.2. HRMS (ESI-TOF) $[M + H]^+$ *m/z*: Calcd. for $C_{22}H_{22}BrCl_4N_2OSi$ 576.9433, found: 576.9428 (Figure S16).

2.2.16. 2″-(4-((Tert-Butyldimethylsilyl)oxy)phenyl)-3′,3″,5′,5″-Tetrachloro-4,2′:4′,4″-Terpyridine **31**

Procedure 2.2.14. was used starting from 2-bromo-3,3′,5,5′-tetrachloro-2′-iodo-4,4′-bipyridine **24** (0.143 mmol, 82.5 mg), $Pd(PPh_3)_4$ (0.007 mmol, 8.3 mg), 4-pyridine boronic acid (0.215 mmol, 31 mg) and K_3PO_4 (0.215 mmol, 46 mg). After purification by chromatography on silica gel (pentane/ethyl acetate 7/3), compound **31** was obtained (60 mg, 73%). Colorless syrup. ^{1}H NMR (500 MHz, $CDCl_3$) δ 8.80 (s, 1H), 8.78 (d, J = 5.5 Hz, 2H), 8.74 (s, 1H), 8.76–8.66 (m, 4H), 6.95 (d, J = 8.5 Hz, 2H), 1.00 (s, 9H), 0.24 (s, 6H). ^{13}C NMR (126 MHz, $CDCl_3$) δ 157.1, 155.9, 153.2, 150.1, 147.9, 147.3, 144.7, 142.9, 141.8, 131.09, 131.05, 130.1, 129.5, 128.7, 128.6, 124.0, 120.0, 25.8, 18.4, −4.2. HRMS (ESI-TOF) $[M + H]^+$ *m/z*: Calcd. for $C_{27}H_{26}Cl_4N_3OSi$ 576.0594, found: 576.0589 (Figure S17).

2.2.17. 4-(3′,3″,5′,5″-Tetrachloro-[4,2′:4′,4″-Terpyridin]-2″-yl)phenol **32**

2″-(4-((Tert-butyldimethylsilyl)oxy)phenyl)-3′,3″,5′,5″-tetrachloro-4,2′:4′,4″-terpyridine **31** (0.078 mmol, 45 mg) was dissolved in THF (2 mL) and the solution was cooled to 0 °C. A tetra-butylammonium fluoride (TBAF) solution (1M in THF, 0.117 mmol, 117 µL) was slowly added and the mixture was stirred at 0 °C for 30 min. After addition of a saturated solution of NH_4Cl (1 mL), the temperature was raised to ambient. Water was added (5 mL) and the mixture was extracted with CH_2Cl_2 (3 × 10 mL). The organic phase was washed

with brine, dried over $MgSO_4$, filtered and concentrated. After filtration on silica gel (ethyl acetate), compound **32** was obtained (36 mg, 100%). White solid, mp 254–256 °C. ^{1}H NMR (500 MHz, DMSO-*d6*) δ 9.998 (broad s, 1H), 9.11 (s, 1H), 8.99 (s, 1H), 8.77 (d, J = 6.0 Hz, 2H), 7.73 (d, J = 6.0 Hz, 2H), 7.62 (d, J = 9.0 Hz, 2H), 6.90 (d, J = 9.0 Hz, 2H). ^{13}C NMR (126 MHz, DMSO-*d6*) δ 158.8, 155.4, 153.1, 150.0, 148.2, 147.5, 143.9, 142.0, 141.1, 131.1, 130.2, 128.4, 127.6, 127.4, 127.2, 115.1. HRMS (ESI-TOF) $[M + H]^+$ *m/z*: Calcd. for $C_{21}H_{12}Cl_4N_3O$ 461.9729, found: 461.9701 (Figure S18).

2.3. Single Crystal X-ray Diffraction

2.3.1. Crystallizations and Analysis

Suitable crystals of compounds **13**, **18** and **24** were obtained by slow evaporation of a dichloromethane/hexane (1:1) solution. The solid-state structures were determined by single crystal X-ray diffraction at low temperature (T = 100 K).

2.3.2. Crystal Data

CCDC 2077648, 2077649 and 2077650 contains the supplementary crystallographic data for this paper. These data can be obtained free of charge via http://www.ccdc.cam.ac.uk/conts/retrieving.html (accessed on 14 April 2021) (or from the CCDC, 12 Union Road, Cambridge CB2 1EZ, UK; Fax: +44 1223 336033; E-mail: deposit@ccdc.cam.ac.uk).

Crystal Data for **24** $C_{10}H_2BrCl_4IN_2$ (M = 498.75 g/mol): Monoclinic, space group $P2_1/c$ (no. 14), a = 7.9297(2) Å, b = 15.6388(4) Å, c = 11.4938(3) Å, β =105.632(2)°, V = 1372.64(6) Å^3, Z = 4, T = 100(2) K, μ(MoKα) = 6.002 mm^{-1}, D_{calc} = 2.413 g/cm^3, 51767 reflections measured ($2.254° \leq \Theta \leq 36.150°$), 6552 unique ($R_{int}$ = 0.0298), which were used in all calculations. The final R_1 was 0.0239 ($I > 2\sigma(I)$) and wR2 was 0.0548 (all data). CCDC 2077649.

Crystal Data for **18** $C_{11}H_3Cl_4N_3$ (M = 334.96 g/mol): Monoclinic, space group $P2_1/c$ (no. 14), a = 7.2662(2) Å, b = 12.0325(4) Å, c = 14.4319(5) Å, β = 93.491(3)°, V = 1259.45(7) Å^3, Z = 4, T = 100(2) K, μ(MoKα) = 0.931 mm^{-1}, D_{calc} = 1.767 g/cm^3, 48102 reflections measured ($2.205° \leq \Theta \leq 33.667°$), 5000 unique ($R_{int}$ = 0.0424), which were used in all calculations. The final R_1 was 0.0323 ($I > 2\sigma(I)$) and wR2 was 0.0732 (all data). CCDC 2077650.

Crystal Data for **13** $C_{10}H_4Cl_4N_2$ (M = 309.95 g/mol): Monoclinic, space group $P2_1/c$ (no. 14), a = 7.2697(2) Å, b = 11.5462(3) Å, c = 14.0808(4) Å, β = 97.804(3)°, V = 1170.96(6) Å^3, Z = 4, T = 100(2) K, μ(MoKα) = 0.991 mm^{-1}, D_{calc} = 1.758 g/cm^3, 48887 reflections measured ($2.290° \leq \Theta \leq 37.162°$), 6021 unique ($R_{int}$ = 0.0444), which were used in all calculations. The final R_1 was 0.0384 ($I > 2\sigma(I)$) and wR2 was 0.0840 (all data). CCDC 2077648.

2.4. Isolated Molecule Calculations

Molecular structures of **24**, **18** and **13** were optimized with Gaussian09 software at DFT level of theory using the B3LYP functional completed with D3 dispersion correction and the Def2TZVPP basis set. Frequency calculations were performed in order to check that true energy minimum were obtained. Electrostatic maps (Figure 2, Figures S31 and S32) were drawn using the AIMAll software, and locations of ESP extrema $V_{S,max}$ were searched using MultiWFN program (Table S4). Integrated atomic charges (AIMAll) are depicted on Figures S33–S35.

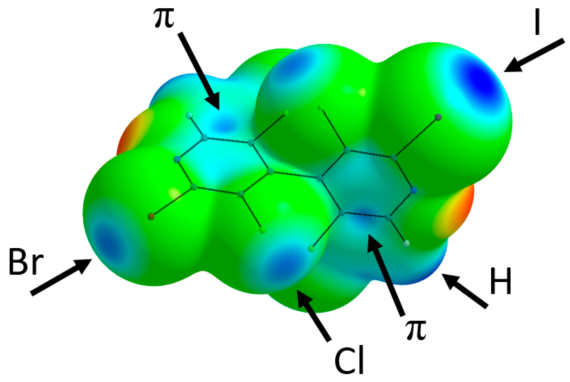

Figure 2. Electrostatic potential mapped on the ρ = 0.002 a.u. electron density isosurface of **24**. Coloring from red = −0.05 a.u. to blue = +0.05 a.u. Black arrows point to some representative electropositive σ- and π-holes.

3. Results

3.1. Improved Synthesis of 3,3′,5,5′-Tetrachloro-4,4′-Bipyridine **10**

The starting 4,4′-bipyridine **10** was already prepared by us with 44% yield by dimerization of 3,5-dichlopyridine **11** [22]. When the synthesis was reproduced on large scale (50 mmol), the yield was improved to 50%. Moreover, during the chromatographic purification, the more polar non-rearomatized compound **12** was also isolated with 40% yield. Compound **12** could be oxidized with I_2 in ethyl acetate at room temperature for 12 h, furnishing **10** with 90% yield. Overall, the yield of **10** in the dimerization process could be increased to 82% yield (Scheme 1).

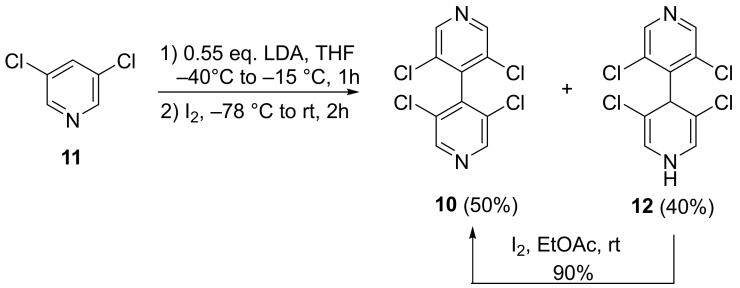

Scheme 1. Improved synthesis of 3,3′,5,5′-tetrachloro-4,4′-bipyridine **10**.

3.2. Desymmetrization of 3,3′,5,5′-Tetrachloro-4,4′-Bipyridine **10**

The mono *N*-oxidation of 4,4′-bipyridine **10** was performed using 1 equivalent of *m*-CPBA in CH_2Cl_2 (0.2 M) at room temperature. After treatment using NaOH 1M to remove the benzoic acid, the crude mixture was purified by chromatography on silica gel to give the expected mono-oxidized 4,4′-bipyridine **13** with 54% yield. Unreacted 4,4′-bipyridine **10** (23%) as well as doubly oxidized 4,4′-bipyridine **14** (23%) were also obtained after the purification. Based on the recovery of the starting 4,4′-bipyridine **10**, the yield of **14** was of 75%. The *N*-oxide **13** could be further transformed to the pentahalogenated 4,4′-bipyridine **15** in very good yields by using oxalyl bromide with Et_3N in CH_2Br_2 at low temperature [23], and to the cyano derivative **16** by using TMSCN/Et_3N in refluxing dioxane [24] (Scheme 2).

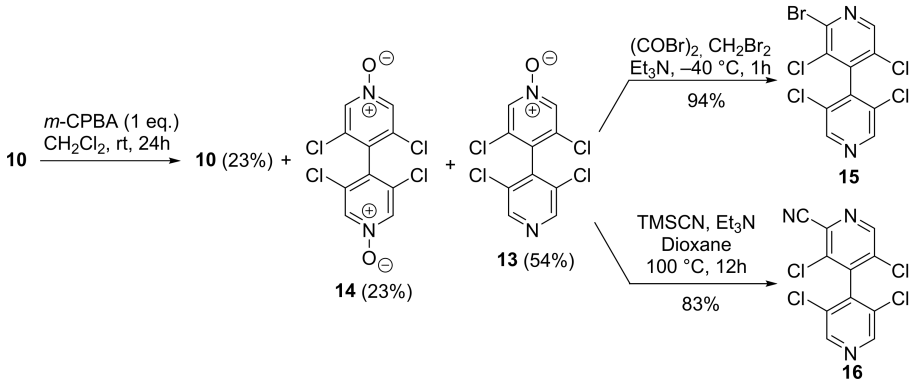

Scheme 2. Mono-oxidation of 4,4′-bipyridine **10** and its functionalization.

3.3. New Chiral Non-Symmetrical 4,4′-Bipyridines Based on the 3,3′,5,5′-Tetrachloro-4,4′-Bipyridine Core

4,4′-Bipyridines **15** and **16** were submitted to a new sequence of *N*-oxidation/halogenation in order to access to novel chiral non-symmetrical 4,4′-bipyridines. Thus, regioselective *N*-oxidation of the less substituted ring of **15** and **16** furnished, respectively, 4,4′-bipyridine *N*-oxides **17** and **18** in high yields. Chlorination of *N*-oxides **17** and **18** using oxalyl chloride with Et_3N in CH_2Cl_2 at low temperature [23] afforded 4,4′-bipyridines **19** and **20** in good yields. Alternatively, *N*-oxide **17** was transformed by a copper-catalyzed Finkelstein reaction [25] to the iodinated 4,4′-bipyridine *N*-oxide **21** which was further submitted to the chlorination to provide 4,4′-bipyridine **22**. *N*-oxides **18** and **21** were also brominated as described in Scheme 2 to give two other chiral non-symmetrical 4,4′-bipyridines **23** and **24** in good yields (Scheme 3). Finally, 4,4′-bipyridine **21** was transformed in good yield to the iodinated 4,4′-bipyridine **25** by using TMSCN/Et_3N in refluxing dioxane.

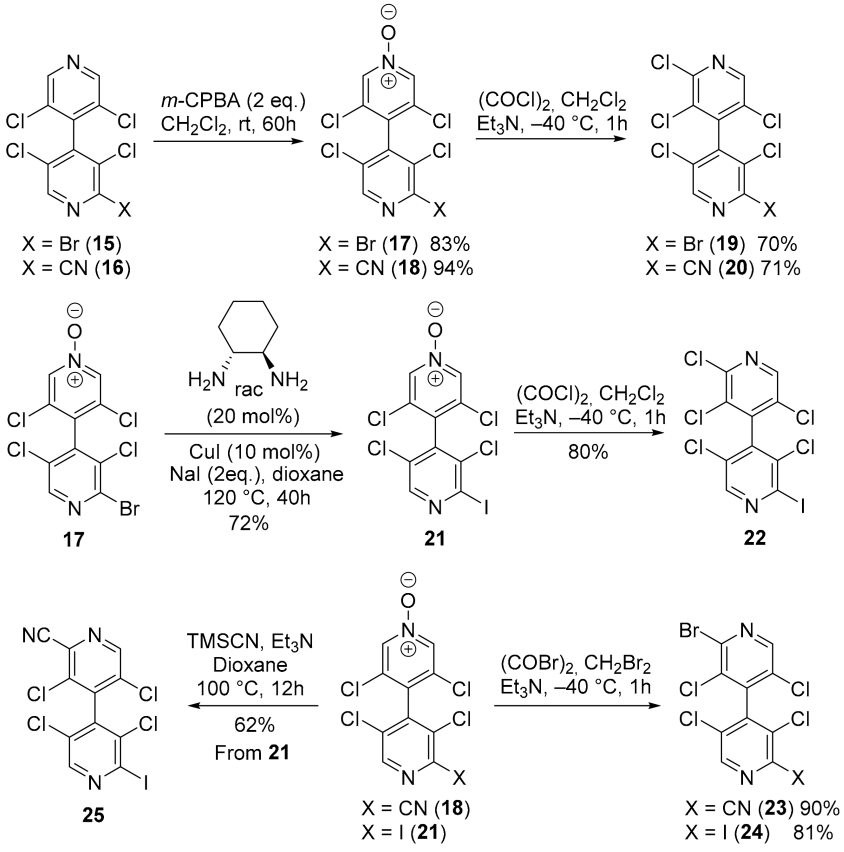

Scheme 3. Synthesis of six new chiral non-symmetrical 4,4′-bipyridines.

3.4. Cross-Coupling Reactions with 4,4′-Bipyridine **24**

4,4′-Bipyridine **24** bearing two different halogens (Br and I) in 2 and 2′-positions was chosen to perform selective cross-coupling reactions. In particular, 4,4′-bipyridines **28** and **30,** which were recently described as good transthyretin fibrillogenesis inhibitors [17], could be obtained in excellent yields and with very high purity by successive Suzuki and Finkelstein reactions, followed by silyl group deprotection in the case of **30**. Moreover, their enantiomers could be separated by HPLC on chiral stationary phase [26,27]. High selectivity for mono-coupling products **26** and **27** was obtained by using the Suzuki coupling [28] with one equivalent of arylboronic acid, letting the C–Br bond untouched for a further coupling reaction such as the copper-catalyzed Finkelstein Br/I exchange [18]. Moreover, a new Suzuki cross-coupling of 4,4′-bipyridine **27** with 4-pyridylboronic acid delivered compound **31,** which, after silyl group deprotection, furnished the chiral 4,4′-bipyridine **32,** bearing two different functional groups (Scheme 4).

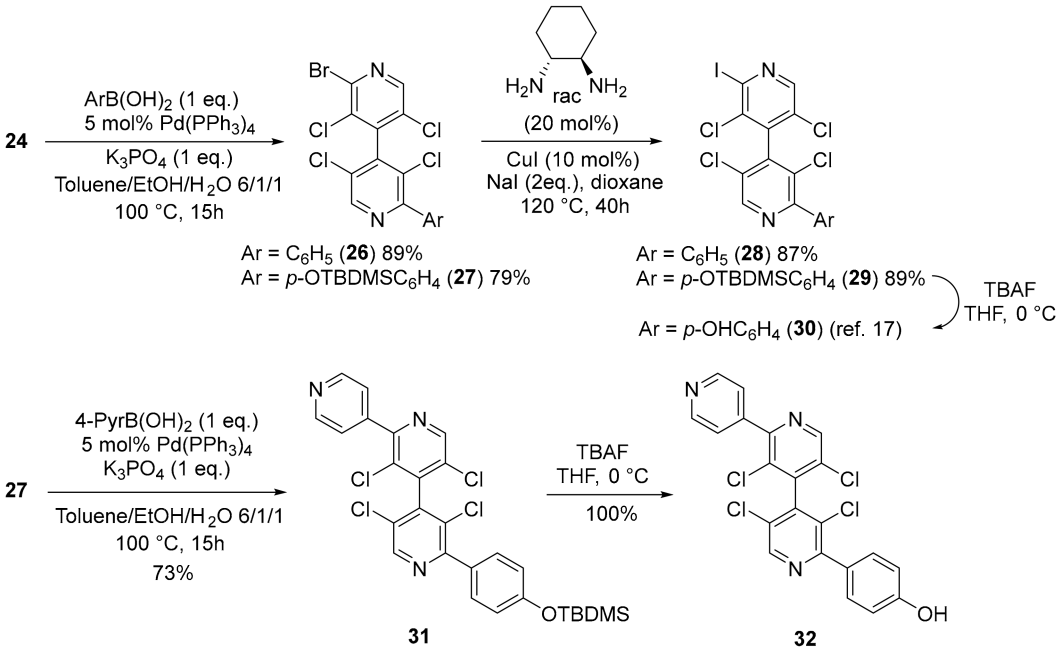

Scheme 4. Cross-coupling reactions with 4,4′-bipyridine **24**.

3.5. X-ray Diffraction Analysis

One non-symmetrical 4,4′-bipyridine (**24**) and two 4,4′-bipyridine *N*-oxydes (**13** and **18**) solid state structures were determined by single X-ray diffraction.

2-Bromo-3,3′,5,5′-tetrachloro-2′-iodo-4,4′-bipyridine **24** crystallizes in $P2_1/c$ space group with one molecule in the asymmetric unit. A positional disorder (corresponding to two different orientations of the molecule) exchanges the Br and I halogen atom positions, the major component having a population of 0.7441(13). According to the energy packing analysis performed with CrystalExplorer software [29], the solid-state structure of **24** is primarily determined by the formation of intermolecular interactions with a predominance of stabilizing dispersion over electrostatic contributions (Table S1, entries 1–6). These contributions involve first the formation of strongly bound dimers centered on an inversion center where $\pi\cdots\pi$ stacking occurs (N7-pyridine interplane distance of 3.272 Å) (Table S1, entry 1 and Figure S19), with a complementary electrostatic interaction between the electropositive C12-H12 group (integrated atomic charges of Q(C12) = +0.59 and Q(H12) = +0.06) and the electronegative crown of Br1 (Q = −0.02), as evidenced from the electrostatic potential mapped on the isodensity molecular surface (Figure 2). In this dimer, the electronegative region about N7 is also near the electropositive area of Cl1, although the σ-hole of the halogen is not optimally oriented (C3-Cl1$\cdots$N7 = 127.59°). The geometry of the next two

intermolecular interactions (x, −y + 3/2, z − 1/2 and 1 + x, −y + 3/2, z + 1/2, Table S1, entries 2–3) can also be understood from electrostatic point of view, since electronegative regions (respectively Cl3 with Q(Cl3) = −0.17 and N1 with Q(N1) = −1.12) are close to electropositive area (respectively C6 with Q(C6) = +0.59 and C12 with Q(C12) = +0.59) (Figures S20 and S21).

The most remarkable feature of the molecular packing is the formation of a four-membered ring involving four I/Br atoms engaged in type-II halogen···halogen bonds (Figure 3). Although the I/Br positional disorder can induce bias in the modeled interatomic distances, these latter show a clear interpenetration of the van der Waals spheres and an interaction geometry typical of type-II hal···hal bonds [30,31] (I1···Br1 = 3.564(2) Å RR = 0.93; C2-I1···Br1 = 170.22(7)°; I1···Br1-C8 = 114.6(1)°; Br1···I1 = 3.716(3) Å RR = 0.97; C8- Br1···I1 = 170.4(1)°; Br1···I1-C2 = 81.45(6)°)). Noticeably, the shortest type-II hal···hal bond is obtained when the σ-hole of the I atom points toward the crown of the Br atom; indeed, the σ-hole is more electropositive for iodine than for bromine (Figure 2 and Table S4), whereas the electronegative crown is more pronounced for the latter. From the intermolecular energy decomposition (Table S1), these interactions appear with predominant electrostatic contribution (entry 7: −1 + x, y, −1 + z), but also with major dispersion contribution along with significant electrostatic contribution (entry 4: 1 − x, 1 − y, 1 − z). This is due to the fact that in the former dimer the molecules are well separated (interacting only through the halogen atoms), whereas in the latter a close proximity of polarizable halogen atoms and aromatic rings is observed.

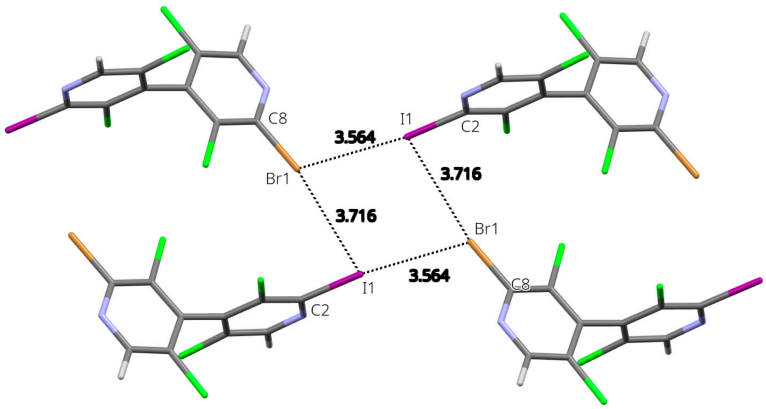

Figure 3. Four-membered ring involving four I/Br atoms (x, y, z; −1 + x, y, −1 + z; −x, 1 − y, −z; 1 − x, 1 − y, 1 − z) engaged in type-II halogen···halogen bonds in the crystal structure of **24**. Representative distances are given in Å. Only the major component disorder is shown.

In order to rationalize the observed positional disorder that involves the iodine and bromine atoms, DFT calculations were undertaken on the isolated tetramer centered about the type-II hal···hal bond's four-membered ring (Figure S36). From the results (Table S5), it appears that the most stable configuration is obtained for the observed largest component disorder (labelled IBrIBr), where the halogen atoms alternate in the sequence Hal1=I, Hal2=Br, Hal3=I, Hal4=Br, as depicted on Figure 3. However, the other configurations are not excessively less stabilizing, with the most unfavorable case (IIII) being only 8.92 kJ/mol higher in energy. Boltzmann populations calculated, taking into account all the possible configurations, finally lead to an equivalent average disorder population of 0.675, in remarkable qualitative agreement with the refined population parameter (0.7441(13)). This may indicate that the observed dissymmetry in the disorder population (i.e., different from 50/50) results from the preferential interaction of the σ-hole of iodine atom toward the crown of bromine at the short distance, at the expense of the reverse situation (interaction of bromine σ-hole toward the crown of iodine).

N-oxides **13** and **18** are isostructural, crystallizing in $P2_1/c$ space group with similar unit cell parameters. Indeed, they present similar crystal packing, with notable differences

only about the substituent in 2 position (-H in **13**, -CN in **18**) (Figures S22 and S23). The analysis of intermolecular interaction energies (Tables S2 and S3) shows that in both structures the main interaction (entry 1) corresponds to the formation of a strong cyclic R2,2(8) hydrogen bond motif about an inversion center, involving the oxygen atom of the *N*-O as the acceptor (Figure 4; **18**: C12-H12· · · O13 = 2.17 Å; 160°; **13**: 2.07 Å; 162°).

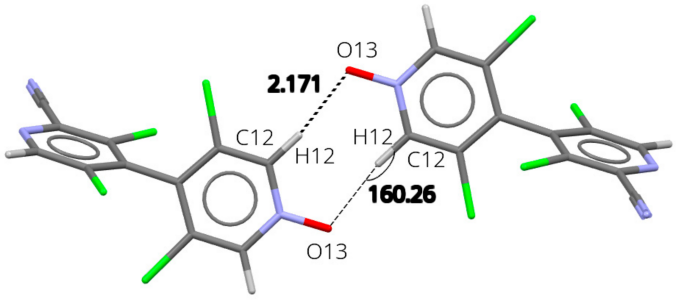

Figure 4. Packing in the solid-state structure of **18**. Interaction between x, y, z, and −1 + x, 1−y, −z molecules. Representative distance is given in Å and angle in °.

The main differences between the two structures concern the next two most intense interactions involving 2 − x, 1 − y,1 − z and 1 − x, 1 − y,1 − z molecules. The first dimer is strongly stabilizing in **18**, with the cyano groups of the two neighboring molecules arranged in a head-to-tail manner (Figure S24), associated with a large electrostatic component (Table S2, entry 2); on the contrary, in **13** the corresponding molecules does not present any contact below van der Waals limit and dispersion is the main stabilizing contribution to the interaction (Table S3, entry 2 and Figure S25). The second dimer (with 1 − x, 1 − y,1 − z, Tables S2 and S3, entry 3) is twice more stabilizing in **18** than in **13** and involves a contact at van der Waals limit between the Cl1 and C14 atoms of the cyano group, the crown of the halogen atom pointing in the direction of the positively charged carbon atom (C3-Cl1· · · C14 = 3.442 Å, 110.04°; Q(C14) = 0.94) (Figure S26); in such a way, both electrostatic and dispersion components are more stabilizing in **18**, while in **13** a C3-Cl1· · · Cl1 contact at van der Waals limit (3.490 Å, 78.83°) implies the crown of both halogen atoms in a unfavorable disposition (Figure S27).

The next interaction (Tables S2 and S3, entry 5; x, −y + 3/2, z − 1/2) evidences also some differences between the structures, although to a lesser extent. In both structures this dimer displays a halogen bond between the σ-hole of Cl3 and the O13 oxygen atom of the *N*-oxide group (**18**: C9-Cl3· · · O13 = 3.152 Å RR = 0.96, 156.54°; **13**: 3.021 Å, RR = 0.92, 157.94°; Figures S28 and S29). However, in **18** a second halogen bond participates in the stabilization, the σ-hole of Cl2 being properly oriented toward the nitrogen atom of the cyano group (C5-Cl2· · · N15 = 3.128 Å, RR = 0.95, 156.31°).

The last significant interaction implies 1 − x, y + 1/2, −z + 1/2 molecule (Tables S2 and S3, entry 6) and is slightly more stabilizing for **13** than for **18** due to a more negative electrostatic contribution. In this latter Cl2 atom presents three contacts at distances smaller than van der Waals limits with this neighbor, namely with N7 (3.179 Å, RR = 0.96), C8 (3.380 Å, RR = 0.98) and C12 (3.426 Å, RR = 0.99), but with an orientation that does not involves the halogen σ-hole (C5-Cl2· · · N7 = 109.10°) (Figure S30). The electrostatic stabilization may then result from the head-to-tail relative orientation of the two molecules which bear a dipole moment parallel to their long N-N axis in the case of **13** (1.87 D), whereas in **18** the molecular dipole moment (3.42 D) is almost parallel to the –CN group. In this situation, the neighboring molecules have almost orthogonal dipole moments and thus a reduced overall electrostatic stabilization.

4. Discussion

The synthesis of 3,3′,5,5′-tetrachloro-4,4′-bipyridine **10** [22] was greatly improved by adjusting the amount of LDA to 0.55 equivalent with regard to 3,5-dichloropyridine

11. Moreover, a large quantity (44%) of dihydropyridine **12** was also isolated during the reaction, confirming the proposed mechanism for the dimerization process [22]. Indeed, after deprotonation of half equivalent of **11**, the nucleophilic lithiated **11-Li** added in 4-position of the remaining half equivalent of **11** to give **12-Li,** which after oxidation with iodine and hydrolysis delivered **10** and non-oxidized **12** (Figure 5A). After purification, dihydropyridine **12** was very stable in the solid state with no noticeable oxidation after three months on the bench at ambient temperature. In acetone solution, a slow oxidation occurred with almost complete formation of 4,4′-bipyridine **10** after 10 days, as shown by ^{1}H NMR (Figure 5B).

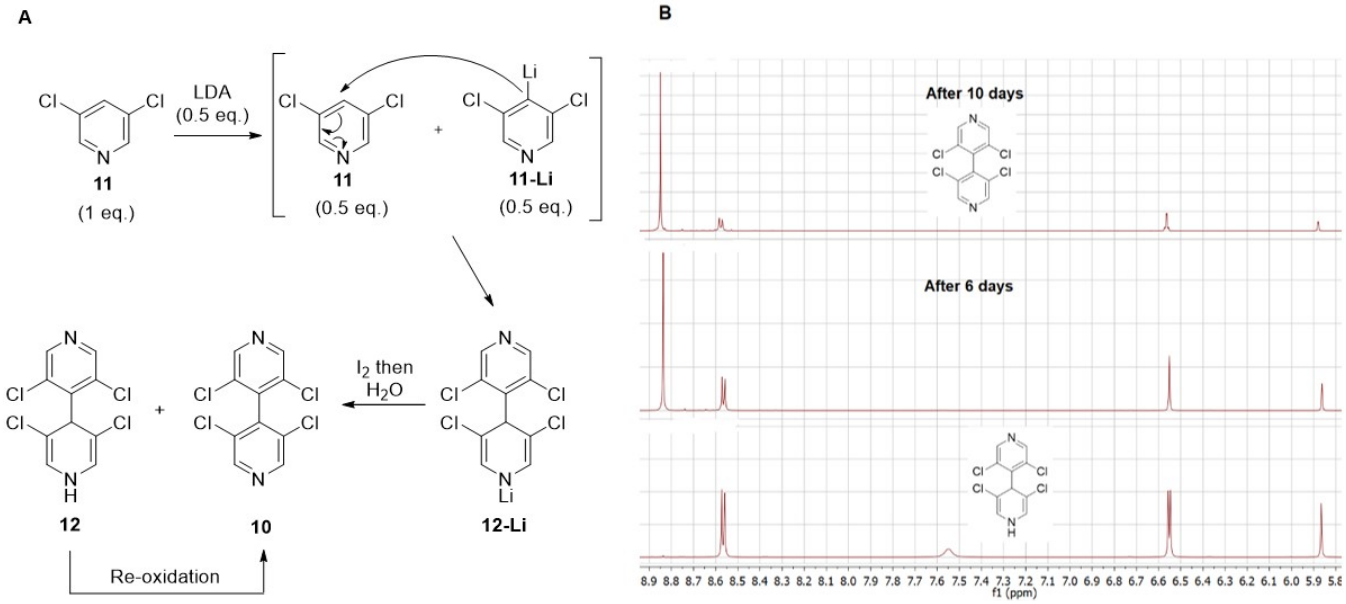

Figure 5. (**A**) Proposed mechanism for the formation of 4,4′-bipyrine **10;** (**B**) ^{1}H NMR spectra showing oxidation of dihydropyridine **12** in acetone over time.

The desymmetrization route of 4,4′-bipyridines used in this study is based on the *N*-oxidation of one of the two pyridine nitrogens in the presence of one equivalent of m-CPBA. *N*-oxidation of electron-deficient pyridines generally requires harsher conditions that necessitate prior *N*-activation with trifluoroacetic acid anhydride [32,33]. As expected, this first *N*-oxidation is not selective; however, the chemical nature of the three compounds of the reaction mixture (starting material with free nitrogens, mono *N*-oxide and bis *N*-oxide) allowed for simple purification with easy recovery of unreacted starting material. The *N*-oxidation of the electron-deficient pentasubstituted 4,4′-bipyridines **15** and **16** was highly selective with no formation of the bis *N*-oxide. The high selectivity of the reaction is due to both electronic and steric factors. Indeed, the trisubstituted pyridine ring is electronically impoverished by the three electron-withdrawing groups (Cl, Cl and Br or CN) and the *N*-pyridine is sterically hindered by the substituent in 2-position (Br or CN).

The choice of the pyridine *N*-oxides in our synthesis was also guided by the numerous known methodologies for their functionalization [21]. Halogenation and cyanation of 4,4′-bipyridine *N*-oxides used in this work are examples of such reactions which efficiently provided 4,4′-bipyridines functionalized in 2-position with Cl, Br and CN. A general mechanism can be proposed for these transformations (Figure 6). After activation of the *N*-oxide by $(COCl)_2$, $(COBr)_2$ or TMSCN, the intermediate may evolve following two different paths. In path a, the generated nucleophile during the first step ($X^- = Cl^-$, Br^- or CN^-) attacks the carbon in 2-position followed by base-assisted elimination of RO^- to give the functionalized pyridine. In path b, the deprotonation of the acidic hydrogen in 2-position first occurs to generate a carbene intermediate which is trapped by the nucleophile with concomitant elimination of RO^-.

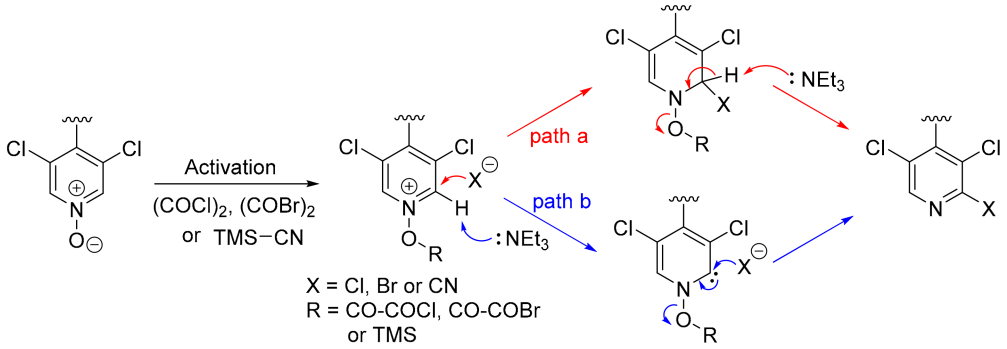

Figure 6. Proposed mechanism for the functionalization of pyridine *N*-oxides.

The installed functions in 2,2′-positions represent a potential entry to new functional groups by nucleophilic substitution of the chlorine, hydrolysis of the cyano group and cross-coupling reaction with the C-Br bond. In the latter case, we have used the copper-catalyzed Finkelstein reaction to exchange bromine by iodine, and the Suzuki reaction to introduce aryl groups in 2-positions. In this regard, 4,4′-bipyridine **24** possessing both bromine and iodine in 2,2′-positions is a compound of choice in order to selectively introduce two different aryl groups on the 3,3′,5,5′-tetrachloro-4,4′-bipyridine scaffold. This was highlighted by the synthesis of 4,4′-bipyridine **32** whose supramolecular arrangement in solution and in the solid state is currently under investigation in our laboratory.

5. Conclusions

A new methodology for the synthesis of chiral non-symmetrical 4,4′-bipyridines was developed. It is based on the successive functionalization of 2- and 2′-positions of 4,4′-bipyridines by using the sequence *N*-oxidation then halogenation or cyanation. Starting from 3,3′,5,5′-tetrachloro-4,4′-bipyridine, all the six possible non-symmetrical isomers bearing Cl, Br, I or CN in 2- and 2′-positions were efficiently prepared. The isomer bearing bromine and iodine was used as the key component for the improved synthesis of biologically active 2-iodinated 4,4′-bipyridines and for the preparation of 4,4′-bipyridines with two different aryl groups in 2- and 2′-positions. This work opens new directions toward the synthesis of non-symmetrical ligands for the design of supramolecular materials, such as coordination polymers and metal-organic frameworks (MOFs).

Supplementary Materials: The following are available online at https://www.mdpi.com/article/10.3390/compounds1020006/s1, Figure S1: 3,3′,5,5′-Tetrachloro-1,4-dihydro-4,4′-bipyridine (**12**), Figure S2: 3,3′,5,5′-Tetrachloro-[4,4′-bipyridine] 1-oxide (**13**), Figure S3: 3,3′,5,5′-Tetrachloro-[4,4′-bipyridine] 1,1′-dioxide (**14**), Figure S4: 2-Bromo-3,3′,5,5′-tetrachloro-4,4′-bipyridine (**15**), Figure S5: 3,3′,5,5′-Tetrachloro-[4,4′-bipyridine]-2-carbonitrile (**16**), Figure S6: 2-Bromo-3,3′,5,5′-tetrachloro-[4,4′-bipyridine] 1-oxide (**17**), Figure S7: 3,3′,5,5′-Tetrachloro-2′-cyano-[4,4′-bipyridine] 1-oxide (**18**), Figure S8: 2-Bromo-2′,3,3′,5,5′-pentachloro-4,4′-bipyridine (**19**), Figure S9: 2′,3,3′,5,5′-Pentachloro-[4,4′-bipyridine]-2-carbonitrile (**20**), Figure S10: 3,3′,5,5′-Tetrachloro-2′-iodo-[4,4′-bipyridine] 1-oxide (**21**), Figure S11: 2,3,3′,5,5′-Pentachloro-2′-iodo-4,4′-bipyridine (**22**), Figure S12: 2′-Bromo-3,3′,5,5′-tetrachloro-[4,4′-bipyridine]-2-carbonitrile (**23**), Figure S13: 2-Bromo-3,3′,5,5′-tetrachloro-2′-iodo-4,4′-bipyridine (**24**), Figure S14: 3,3′,5,5′-Tetrachloro-2′-iodo-[4,4′-bipyridine]-2-carbonitrile (**25**), Figure S15: 2-Bromo-3,3′,5,5′-tetrachloro-2′-phenyl-4,4′-bipyridine (**26**), Figure S16: 2-Bromo-2′-(4-((tert-butyldimethylsilyl)oxy)phenyl)-3,3′,5,5′-tetrachloro-4,4′-bipyridine (**27**), Figure S17: 2″-(4-((Tert-butyldimethylsilyl)oxy)phenyl)-3′,3″,5′,5″-tetrachloro-4,2′:4′,4″-terpyridine (**31**), Figure S18: 4-(3′,3″,5′,5″-Tetrachloro-[4,2′:4′,4″-terpyridin]-2″-yl)phenol (32), Figure S19: Packing in the solid-state structure of **24**. Interaction between x, y, z, and 2 − x, 1 − y, 1 − z molecules. Representative distance is given in Å. Only the major component disorder is shown, Figure S20: Packing in the solid-state structure of **24**. Interaction between x, y, z, and x, −y + 3/2, z − 1/2 molecules. Representative distance is given in Å. Only the major component disorder is shown, Figure S21: Packing in the solid-state structure of **24**. Interaction between x, y, z, and 1 + x, −y + 3/2, z + 1/2 molecules. Representative distance is given in Å. Only the major component disorder is shown, Figure S22:

Superimposition of the molecular environment about a central molecule (displayed as ball and sticks) showing the isostructural relationship between **18** (colored as atom type) and **13** (light gray), Figure S23: Focus on the region centered on –CN group in **18**, showing the largest differences between **18** (colored as atom type) and **13** (light gray) crystal structures, Figure S24: Packing in the solid-state structure of **18**. Interaction between x, y, z, and $2-x, 1-y, 1-z$ molecules. Representative distances are given in Å, Figure S25: Packing in the solid-state structure of **13**. Interaction between x, y, z, and $2-x, 1-y, 1-z$ molecules. Representative distance is given in Å, Figure S26: Packing in the solid-state structure of **18**. Interaction between x, y, z, and $1-x, 1-y, 1-z$ molecules. Representative distances are given in Å, Figure S27: Packing in the solid-state structure of **13**. Interaction between x, y, z, and $1+x, -y+3/2, z+1/2$ molecules. Representative distances are given in Å, Figure S28: Packing in the solid-state structure of **18**. Interaction between x, y, z, and $x, -y+3/2, z-1/2$ molecules. Representative distances are given in Å, Figure S29: Packing in the solid-state structure of **13**. Interaction between x, y, z, and $x, -y+3/2, z-1/2$ molecules. Representative distances are given in Å, Figure S30: Packing in the solid-state structure of **13**. Interaction between x, y, z, and $1-x, y+1/2, -z+1/2$ molecules. Representative distances are given in Å, Figure S31: Electrostatic potential mapped on the ρ = 0.002 a.u. electron density isosurface of **13**. Coloring from red = −0.05 a.u. to blue = +0.05 a.u., Figure S32: Electrostatic potential mapped on the ρ = 0.002 a.u. electron density isosurface of **18**. Coloring from red = −0.05 a.u. to blue = +0.05 a.u., Figure S33: Integrated Bader atomic charges for isolated 24 molecule, Figure S34: Integrated Bader atomic charges for isolated **13** molecule, Figure S35: Integrated Bader atomic charges for isolated **18** molecule, Figure S36: Tertamer extracted from the experimental structure of **24** and used for the modeling of I/Br substation disorder. HalX/HalX′ are I/Br or Br/I, Table S1: Intermolecular interaction energies (kJ/mol) in the packing of solid state structure of **24**. R is the distance between molecular centroids (mean atomic position) in Å, Table S2: Intermolecular interaction energies (kJ/mol) in the packing of solid state structure of **18**. Largest differences between **18** and **13** are highlighted in bold. R is the distance between molecular centroids (mean atomic position) in Å, Table S3. Intermolecular interaction energies (kJ/mol) in the packing of solid state structure of **13** Largest differences between **18** and **13** are highlighted in bold. R is the distance between molecular centroids (mean atomic position) in Å, Table S4. Electrostatic potential maxima ($V_{S,max}$; kcal/mol) on the molecular surface ρ = 0.002 a.u. of **24**, Table S5: Type-II hal$\cdots$hal bonds four membered ring tetramer relative energies. Hal1-2-3-4 numbering corresponds to Figure S18.

Author Contributions: Conceptualization, V.M. and P.P.; methodology, V.M.; X-ray analysis, E.A. and E.W.; data curation, V.M.; writing—original draft preparation, V.M.; writing—review and editing, all authors. All authors have read and agreed to the published version of the manuscript.

Funding: This research received no external funding.

Data Availability Statement: All the data are given in the article and in the associated supporting information.

Acknowledgments: We thank University of Strasbourg and CNRS for financial support. "The Plateforme de Mesures de Diffraction et Diffusion des rayons X of Université de Lorraine" is thanked for providing access to crystallographic facilities. The EXPLOR mesocentre is thanked for computing facilities (Project 2019CPMXX0984).

Conflicts of Interest: The authors declare no conflict of interest.

References

1. Biradha, K.; Sarkar, M.; Rajput, L. Crystal engineering of coordination polymers using 4,4′-bipyridine as a bond between transition metal atoms. *Chem. Commun.* **2006**, *40*, 4169–4179. [CrossRef] [PubMed]
2. Striepe, L.; Baumgartner, T. Viologens and their application as functional materials. *Chem. Eur. J.* **2017**, *23*, 16924–16940. [CrossRef] [PubMed]
3. Papadakis, R. Mono-and di-quaternized 4,4′-bipyridine derivatives as key building blocks for medium- and environment-responsive compounds and materials. *Molecules* **2019**, *25*, 1. [CrossRef] [PubMed]
4. Chelucci, G.; Thummel, R.P. Chiral 2,2′-bipyridines, 1,10-phenanthrolines, and 2,2′:6′,2″-terpyridines: Syntheses and applications in asymmetric homogeneous catalysis. *Chem. Rev.* **2002**, *102*, 3129–3170. [CrossRef]
5. Fletcher, N.C. Chiral 2,2′-bipyridines: Ligands for asymmetric induction. *J. Chem. Soc. Perkin Trans. 1* **2002**, *16*, 1831–1842. [CrossRef]

6. Bednářová, E.; Malatinec, S.; Kotora, M. Applications of Bolm's ligand in enantioselective synthesis. *Molecules* **2020**, *25*, 958. [CrossRef]
7. Sbircea, L.; Sharma, N.D.; Clegg, W.; Harrington, R.W.; Horton, P.N.; Hursthouse, M.B.; Apperley, D.C.; Boyd, D.R.; James, S.L. Chemoenzymatic synthesis of chiral 4,4′-bipyridyls and their metal–organic frameworks. *Chem. Commun.* **2008**, *43*, 5538–5540. [CrossRef]
8. Jouaiti, A.; Hosseini, M.W.; Kyritsakas, N. Non-centrosymmetric packing of 1-d coordination networks based on chirality. *Chem. Commun.* **2002**, *17*, 1898–1899. [CrossRef]
9. Mamane, V.; Aubert, E.; Peluso, P.; Cossu, S. Synthesis, resolution, and absolute configuration of chiral 4,4′-bipyridines. *J. Org. Chem.* **2012**, *77*, 2579–2583. [CrossRef]
10. Rang, A.; Engeser, M.; Maier, N.M.; Nieger, M.; Lindner, W.; Schalley, C.A. Synthesis of axially chiral 4,4′-bipyridines and their remarkably selective self-assembly into chiral metallo-supramolecular squares. *Chem. Eur. J.* **2008**, *14*, 3855–3859. [CrossRef]
11. Aubert, E.; Abboud, M.; Doudouh, A.; Durand, P.; Peluso, P.; Ligresti, A.; Vigolo, B.; Cossu, S.; Pale, P.; Mamane, V. Silver(I) coordination polymers with 3,3′,5,5′-tetrasubstituted 4,4′-bipyridine ligands: Towards new porous chiral materials. *RSC Adv.* **2017**, *7*, 7358–7367. [CrossRef]
12. Peluso, P.; Mamane, V.; Aubert, E.; Dessì, A.; Dallocchio, R.; Dore, A.; Pale, P.; Cossu, S. Insights into halogen bond-driven enantioseparations. *J. Chromatogr. A* **2016**, *1467*, 228–238. [CrossRef]
13. Peluso, P.; Mamane, V.; Dallocchio, R.; Dessì, A.; Villano, R.; Sanna, D.; Aubert, E.; Pale, P.; Cossu, S. Polysaccharide-based chiral stationary phases as halogen bond acceptors: A novel strategy for detection of stereoselective σ-hole bonds in solution. *J. Sep. Sci.* **2018**, *41*, 1247–1256. [CrossRef]
14. Peluso, P.; Gatti, C.; Dessì, A.; Dallocchio, R.; Weiss, R.; Aubert, E.; Pale, P.; Cossu, S.; Mamane, V. Enantioseparation of fluorinated 3-arylthio-4,4′-bipyridines: Insights into chalcogen and π-hole bonds in high-performance liquid chromatography. *J. Chromatogr. A* **2018**, *1567*, 119–129. [CrossRef]
15. Peluso, P.; Dessì, A.; Dallocchio, R.; Sechi, B.; Gatti, C.; Chankvetadze, B.; Mamane, V.; Weiss, R.; Pale, P.; Aubert, E.; et al. Enantioseparation of 5,5′-dibromo-2,2′-dichloro-3-selanyl-4,4′-bipyridines on polysaccharide-based chiral stationary phases: Exploring chalcogen bonds in liquid-phase chromatography. *Molecules* **2021**, *26*, 221. [CrossRef]
16. Weiss, R.; Aubert, E.; Peluso, P.; Cossu, S.; Pale, P.; Mamane, V. Chiral chalcogen bond donors based on the 4,4′-bipyridine scaffold. *Molecules* **2019**, *24*, 4484. [CrossRef]
17. Dessì, A.; Peluso, P.; Dallocchio, R.; Weiss, R.; Andreotti, G.; Allocca, M.; Aubert, E.; Pale, P.; Mamane, V.; Cossu, S. Rational design, synthesis, characterization and evaluation of iodinated 4,4′-bipyridines as new transthyretin fibrillogenesis inhibitors. *Molecules* **2020**, *25*, 2213. [CrossRef]
18. Mamane, V.; Peluso, P.; Aubert, E.; Cossu, S.; Pale, P. Chiral hexahalogenated 4,4′-bipyridines. *J. Org. Chem.* **2016**, *81*, 4576–4587. [CrossRef]
19. Foulger, N.J.; Wakefield, B.J. Polyhalogenoaromatic compounds. XXIX. Hexachloro-5,5′-dilithio-4,4′-bipyridine as an intermediate for organometallic and organic syntheses. *J. Organomet. Chem.* **1974**, *69*, 161–167. [CrossRef]
20. Mamane, V.; Aubert, E.; Peluso, P.; Cossu, S. Lithiation of prochiral 2,2′-dichloro-5,5′-dibromo-4,4′-bipyridine as a tool for the synthesis of chiral polyhalogenated 4,4′-bipyridines. *J. Org. Chem.* **2013**, *78*, 7683–7689. [CrossRef]
21. Kutasevich, A.V.; Perevalov, V.P.; Mityanov, V.S. Recent progress in non-catalytic C–Hunctionalization of heterocyclic *N*-oxides. *Eur. J. Org. Chem.* **2021**, *2021*, 357–373. [CrossRef]
22. Abboud, M.; Mamane, V.; Aubert, E.; Lecomte, C.; Fort, Y. Synthesis of polyhalogenated 4,4′-bipyridines via a simple dimerization procedure. *J. Org. Chem.* **2010**, *75*, 3224–3231. [CrossRef] [PubMed]
23. Chen, Y.; Huang, J.; Hwang, T.L.; Chen, M.J.; Tedrow, J.S.; Farrell, R.P.; Bio, M.M.; Cui, S. Highly regioselective halogenation of pyridine *N*-oxide: Practical access to 2-halo-substituted pyridines. *Org. Lett.* **2015**, *17*, 2948–2951. [CrossRef] [PubMed]
24. Carson, M.W.; Giese, M.W.; Coghlan, M.J. An intra/intermolecular Suzuki sequence to benzopyridyloxepines containing geometrically pure exocyclic tetrasubstituted alkenes. *Org. Lett.* **2008**, *10*, 2701–2704. [CrossRef] [PubMed]
25. Klapars, A.; Buchwald, S.L. Copper-catalyzed halogen exchange in aryl halides: An aromatic Finkelstein reaction. *J. Am. Chem. Soc.* **2002**, *124*, 14844–14845. [CrossRef] [PubMed]
26. Peluso, P.; Sechi, B.; Lai, G.; Dessì, A.; Dallocchio, R.; Cossu, S.; Aubert, E.; Weiss, R.; Pale, P.; Mamane, V.; et al. Comparative enantioseparation of chiral 4,4′-bipyridine derivatives on coated and immobilized amylose-based chiral stationary phases. *J. Chromatogr. A* **2020**, *1625*, 461303. [CrossRef] [PubMed]
27. Dallocchio, R.; Sechi, B.; Dessì, A.; Chankvetadze, B.; Cossu, S.; Mamane, V.; Weiss, R.; Pale, P.; Peluso, P. Enantioseparations of polyhalogenated 4,4′-bipyridines on polysaccharide-based chiral stationary phases and molecular dynamics simulations of selector–selectand interactions. *Electrophoresis* **2021**. [CrossRef] [PubMed]
28. Perdomo Rivera, R.; Ehlers, P.; Ohlendorf, L.; Torres Rodríguez, E.; Villinger, A.; Langer, P. Chemoselective synthesis of arylpyridines through Suzuki–Miyaura cross-coupling reactions. *Eur. J. Org. Chem.* **2018**, *8*, 990–1003. [CrossRef]
29. Turner, M.J.; McKinnon, J.J.; Wolff, S.K.; Grimwood, D.J.; Spackman, P.R.; Jayatilaka, D.; Spackman, M.A. CrystalExplorer17 (2017). University of Western Australia. Available online: https://hirshfeldsurface.net (accessed on 26 February 2021).
30. Desiraju, G.R.; Parthasarathy, R. The nature of halogen···halogen interactions: Are short halogen contacts due to specific attractive forces or due to close packing of nonspherical atoms? *J. Am. Chem. Soc.* **1989**, *111*, 8725–8726. [CrossRef]
31. Metrangolo, P.; Resnati, G. Type II halogen···halogen contacts are halogen bonds. *IUCrJ* **2014**, *1*, 5–7. [CrossRef]

32. Zhu, X.; Kreutter, K.D.; Hu, H.; Player, M.R.; Gaul, M.D. A novel reagent combination for the oxidation of highly electron deficient pyridines to *N*-oxides: Trifluoromethanesulfonic anhydride/sodium percarbonate. *Tetrahedron Lett.* **2008**, *49*, 832–834. [CrossRef]
33. Caron, S.; Do, N.D.; Sieser, J.E. A practical, efficient, and rapid method for the oxidation of electron deficient pyridines using trifluoroacetic anhydride and hydrogen peroxide–urea complex. *Tetrahedron Lett.* **2000**, *41*, 2299–2302. [CrossRef]